I&EC research
Industrial & Engineering Chemistry Research
pubs.acs.org/IECR
Article

MIL-160(Al) as a Candidate for Biogas Upgrading and CO_2 Capture by Adsorption Processes

Mohsen Karimi,* Alexandre Ferreira,* Alírio E. Rodrigues, Farid Nouar, Christian Serre,* and José A. C. Silva*

Cite This: *Ind. Eng. Chem. Res.* 2023, 62, 5216−5229
Read Online

ABSTRACT: The microporous bioderived Al dicarboxylate MIL-160(Al) MOF in its shaped form has been evaluated as a candidate for biogas upgrading (BU) and/or carbon capture and storage (CCS) by studying adsorption isotherms of CO_2, CH_4, and N_2 at 313, 343, and 373 K until 8 bar. The isotherms disclosed the following loading capacities: 4.2 (CO_2), 2.07 (CH_4), and 0.69 (N_2) mol/kg at 5.8 bar and 313 K, which fitted with the dual-site Langmuir model. The linear-driving-force coefficients (LDFs) for CO_2 and CH_4 calculated from uptake rate experiments are in the order of 0.021−0.096 and 0.041−0.165 s^{-1} at 313 K between 0.11 and 2.76 bar, respectively. The Response Surface Methodology (RSM) was also applied to maximize the selectivity for mixtures CO_2/CH_4 and CO_2/N_2 with interest for BU or CCS. Breakthrough curve experiments with mixtures CO_2/CH_4 and CO_2/N_2 at the optimum selectivity conditions were developed and simulated using ASPEN Adsorption. This work clearly demonstrates the potential of MIL-160(Al) to be used in BU- and/or CCS-related applications.

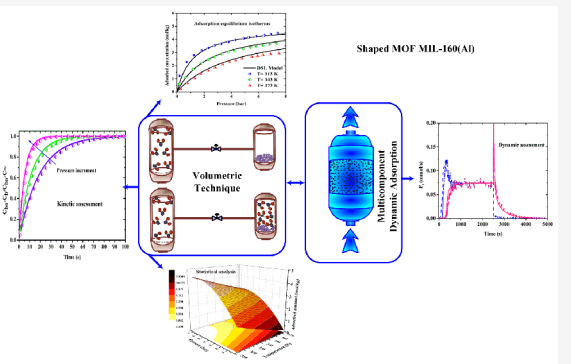

1. INTRODUCTION

Global warming and the requirement to reduce greenhouse gases (GHGs) emissions in the energy sector have been challenging issues in recent decades.[1,2] Undoubtedly, the ascending trend of GHGs stems from human activities including the combustion of coal, oil, and natural gas, which is responsible for more than 80% of CO_2 emissions worldwide.[3,4] According to reports, by the current ascending level of GHGs, climate change will result in 3−5 °C temperature enhancement of the planet at the end of this century,[5,6] which can cause a 95 cm rise in the sea level.[7] Based on the Paris Agreement,[8] the CO_2 emissions shall be restricted to reduce the atmospheric temperature by 2 °C by 2100, which, according to a pragmatic scenario, would require 40−70% CO_2 emission reduction by 2050 and net-zero emissions by 2100. To this end, two main strategies have been proposed by the International Energy Agency (IEA)[9] and the Intergovernmental Panel on Climate Change (IPPC).[10] In this way, based on the BLUE Map Scenario of IEA, the Carbon Capture and Sequestration (CCS) strategy can decrease and control the GHG emissions from the fixed industrial sources, which might result in a 19% reduction in CO_2 emissions by 2050.[11] Accordingly, the fossil fuels of current technologies should be substituted by renewable sources of energy including biogas, solar energy, etc.[12,13] The average growth rate of renewable energies has been 2.0% during the last two decades, and around 11.5% of this growth is attributed to biogas.[14] Currently, Europe is the world leader of biogas development, and its production is expected to reach 30−40% of Europe's total gas consumption by 2050.[14,15] Routinely, biogas as the main output of anaerobic digestion of organic wastes contains carbon dioxide (30−40 vol %), methane (50−70 vol %), and traces of other gases (N_2, H_2, H_2S, etc.);[16] therefore, biogas requires to be upgraded through the separation of CO_2 (biogas upgrading (BU)).[17] Although the biogas upgrading market and technologies are quickly growing, currently, membrane, adsorption, and cryogenic methods are the most employed ones globally. Table 1 represents the typical compositions of commercial biogas derived from anaerobic digestion and landfills.[16,18] Numerous studies have been devoted to develop adsorption processes as efficient and low-cost technologies for BU and CCS.[19] For such purpose, several microporous sorbents, including activated carbons,[20] zeolites,[21] metal−organic frameworks,[22] etc.,[19,23] have been studied. To be employed for large-scale adsorption process design, data including (i) adsorption equilibrium isotherms and the

Received: November 17, 2022
Revised: March 2, 2023
Accepted: March 2, 2023
Published: March 14, 2023

https://doi.org/10.1021/acs.iecr.2c04150
Ind. Eng. Chem. Res. 2023, 62, 5216−5229

Table 1. Typical Compositions of Commercial Biogas Derived from Anaerobic Digestion and Landfill

parameter		biogas from AD	biogas from landfill
composition (% mol)	CH_4	60−70	35−65
	CO_2	30−40	15−40
	H_2O	1−5	1−5
	N_2	0.2	15
	H_2	0	0−3
	heavy carbon	0	0
minimum methane number		135	130
lower heating value (MJ/kg)		23	16
Wobbe index (MJ/Nm^3)		27	18
density (kg/Nm^3)		1.2	1.3

respective heat of adsorption, (ii) kinetics of adsorption, (iii) selectivities, and (iv) cost are of fundamental importance.[24]

Metal−organic frameworks (MOFs), as 2D or 3D micro- or mesoporous coordination polymers, are a class of porous crystalline hybrid materials[25−27] constructed from the association of inorganic nodes (clusters, chains, or layers) and organic linkers (carboxylates, phosphonates, azolates, etc.).[28] Their structure and pore size/shape can easily be tuned by modifying the organic linker, whereas the functional groups, attached to the organic spacer or grafted onto the open metal sites, enable a careful design of the adsorption sites and/or modulation of the hydrophilic/hydrophobic balance.[29] This unique diversity makes MOFs appealing candidates for gas separation and purification with a broad range of functionality for kinetics, thermodynamics, and selectivity.[30] In this way, numerous types of MOFs have been introduced for gas sequestration and storage in the recent years.[31−33] In spite of the abovementioned attractive characteristics, the first generation of MOFs was reported in most cases to be poorly chemically stable and/or produced under high-temperature hydro- or solvothermal conditions using toxic solvents, which precluded their practical use.[34−37] Among numerous efforts reported to date to develop water-stable MOFs using high-valence metal cations (Zr, Ti, Al, Fe, Cr, etc.),[38] some of us reported the Al dicarboxylate MOF denoted as MIL-160(Al) built from the bioderived 2,5-FDCA (furane dicarboxylic acid) ligand. This water-stable hydrophilic MOF was shown to be a promising candidate for a large range of sorption related applications from CO_2 capture postcombustion studies, acid gas separation,[39] separation of olefins,[40] xylenes, branched alkanes,[41] biogas upgrading, and heat pump/chiller applications.[42−44] In addition to its easy ambient pressure green synthesis conditions, a technico-economic cost production analysis at the industrial scale has been recently performed by Severino et al. and revealed that upon upscaling of the 2,5-FDCA ligand for the industrial production of bioplastics, this MOF could be produced at the large scale (e.g. 1 kt/year) with a reasonable cost.[45]

Accordingly, in this work, the capacity of MIL-160(Al) as a candidate for BU and CCS (especially in postcombustion processes) was studied by evaluating the adsorption equilibrium isotherms of carbon dioxide, methane, and nitrogen using a piezometric/volumetric technique between 313 and 373 K. The isotherms were modeled using the dual-site Langmuir (DSL) model, and the isosteric heat of adsorption was evaluated by the Clausius−Clapeyron equation. Afterward, the kinetic data taken from the uptake rate experiments were assessed to calculate lumped mass transfer coefficients (through a simplified solid-phase linear-driving-force rate law (LDF)) using a proper batch piezometric−volumetric adsorber model. Furthermore, the Response Surface Methodology (RSM) was employed for the statistical analysis of the adsorption equilibrium data and respective selectivities for the binary systems CO_2/CH_4 and CO_2/N_2 to derive optimum operating conditions for designing the cyclic adsorption processes. The working capacities were also calculated. Finally, dynamic studies of binary CO_2/CH_4 and CO_2/N_2 adsorption onto shaped MIL-160(Al) in a fixed-bed adsorber were performed by measuring binary breakthrough curves at 313 K and 3 bar, which were also predicted by using ASPEN Adsim using a proper mathematical model, to prove the reliability of the data. In the end, the adsorption characters of MIL-160(Al) were compared with other candidates for BU and CCS processes, and it was proven to be a very competitive sorbent for large-scale applications of CO_2 separation under BU and CCS strategies with regard to its singular specifications including stability, cost, and easy shaping. Accordingly, the results arising from this work are now being used in the development of pressure/temperature swing adsorption processes for BU and CCS under industrial relevant operating conditions.

2. EXPERIMENTAL SECTION

2.1. Materials. A detailed description of the synthesis of MOF MIL-160(Al) granules can be found in ref 44, and here, a short description is presented. This adsorbent, isostructural material from the parent CAU-10(Al)[44] is built up from helicoidal *cis*-chains of $AlO_4(OH)_2$ octahedra connected through 2,5-FDCA ligands, resulting into microporous channels of free aperture of 5−6 Å.[42,44] This MOF can also be made under scalable green ambient pressure conditions with a very good space time yield (>160 kg day^{-1} m^{-3}). Because of its microporous polar character, it was also shown to exhibit an excellent affinity for diverse polar molecules such as CO_2, SO_2, or acetylene. MIL-160(Al) is therefore a suitable candidate for the selective adsorption under precombustion processes such as biogas upgrading.[42,44] The shaping of MIL-160(Al) was carried out through wet granulation using 5 wt % colloidal silica as a binder following a previously reported protocol, leading to mechanically stable millimeter-sized granules (crushing strength of ca. 10 N) with sorption properties close to those of the starting powder.[44]

The characterization of shaped samples was accomplished by N_2 adsorption at 77 K (Figure S1, Supporting Information), including the determination of the Brunauer, Emmett, and Teller (BET) surface area (Table 2), at the University of Malaga-Spain using a Micromeritics ASAP 2020 (V4.02) equipment. Furthermore, the mercury porosimetry evaluation was accomplished by a Micromeritics AutoPore IV 9500, from pressure 0.20 to 61,000.00 psia, to specify the total intrusion volume, pore area, pore diameter, density, and porosity (Table 2). In addition, the employed pure gases such as CO_2, CH_4, and N_2 for the adsorption studies, and also helium (He) as inert gas for regeneration and activation, were supplied by Air Liquide.

2.2. Experimental Measurements. *2.2.1. Volumetric Apparatus.* The adsorption equilibrium isotherms of CO_2, CH_4, and N_2 were measured using an in-house built piezometric/volumetric apparatus fully described elsewhere.[46] Briefly, the unit includes two independent volume cells, one

https://doi.org/10.1021/acs.iecr.2c04150
Ind. Eng. Chem. Res. 2023, 62, 5216−5229

Table 2. Characterization and Textural Properties of Shaped MIL-160(Al)

adsorbent properties		
parameter	numerical values	unit
particle radius	0.001	m
total intrusion volume at 206.4937 MPa	0.22	mL/g
total pore area at 206.4937 MPa	19.45	m^2/g
median pore diameter (volume) at 7.7053 MPa and 0.110 mL/g	1.62	Å
median pore diameter (area) at 119.8197 MPa and 9.728 m^2/g	104.1	Å
average pore diameter (4 V/A)	453.9	Å
bulk density at 0.0037 MPa	1.07	g/mL
apparent (skeletal) density at 206.4937 MPa	1.40	g/mL
surface area[a]	986	m^2/g
micropore area[b]	959	m^2/g
total pore volume	0.379	cm^3/g
micropore volume	0.336	cm^3/g

[a]Surface area determined by the Langmuir method. [b]*t*-plot micropore area.

containing the adsorbent and the other being a reference cell, designed in a batch loop using a circulating pump operating in −100 mbar (vacuum) until 150 bar supplied by Thomas Co. A pressure transducer monitors the pressure in the system with ±0.1% full scale (FS) and the accuracy of ±0.08% BSL, which was provided by Omega Co. The temperature of the adsorption cell was controlled by a chromatographic oven. Also, the temperature in both adsorption and reference cells was continuously assessed by two thermocouples. Furthermore, a vacuum pump (Thomas Co.) provided the required vacuum during the activation procedure. To measure the adsorption equilibrium isotherms, the adsorption cell was first loaded by 0.30 g of shaped MIL-160 (Al). Then, the activation of samples was performed to remove the moisture and impurities by heating the system at the rate of 1 K/min, up to 423 K, under a vacuum and helium (21.8 NmL/min) and keeping the temperature and operating conditions for 12 h. Some specific properties of the experimental unit are presented in Table 3.

2.2.2. Breakthrough Experiments. The dynamic breakthrough experiments for assessment of the potential of MIL-160(Al) for CO_2/CH_4 and CO_2/N_2 separations were accomplished in a fixed-bed adsorber system. In this unit, the outlet gas compositions were tracked by an infrared gas analyzer (Gas Data Ltd., LMSxi Type G4.18, U.K.). Also, the temperature history was recorded using one thermocouple fitted at the middle position of the stainless steel column. In addition, mass flow controllers measured the feed flowrates, whereas the flowrate of the outlet stream was measured by a mass flow meter, all provided by Alicat Scientific. Furthermore, the pressure was controlled using a backpressure regulator by Bronkhorst. Some specific properties of the experimental setup are provided in Table 4. More details regarding this unit can be found elsewhere.[18]

Table 3. Key Details and Specifications of the Volumetric Unit

volumetric unit specifications		
parameter	numerical value	unit
reference volume	44	cm^3
adsorption cell	2.5	cm^3
residual volume	0.8	cm^3
mass of sample		
mass of raw sample	0.302	g
mass of activated sample	0.272	g
general parameters		
ambient temperature	298	K
ambient pressure	1	bar
developed isotherms		
T	313, 343, 373	K
P	0.1−8	bar

Table 4. Key Characteristics of the Dynamic Adsorption Fixed-Bed System

breakthrough unit specifications		
bed characters	numerical values	unit
bed length	6.8	cm
bed internal diameter	2.1	cm
wall thickness	2.54	cm
bulk solid density of adsorbent	463.03	kg/m^3
mass of raw sample	12.2	g
mass of activated sample	10.9	g
interparticle or bed porosity	0.48	m^3_{void}/m^3_{bed}
intraparticle porosity	0.31	m^3_{void}/m^3_{bead}

To accomplish the breakthrough experiments, a fresh adsorbent sample was first activated using a similar protocol as in the volumetric experiments but with the helium flowrate at 327.5 Nml/min. To start the binary experiment of CO_2/CH_4, the column was first saturated with helium; afterward, the feed flow containing 50% CO_2 and 50% CH_4 was injected to the column until steady-state conditions were reached. Afterward, the regeneration process was performed by shifting the inlet flow to pure helium. Further, to accomplish the pseudobinary experiment of CO_2/N_2, the bed was first saturated with nitrogen, and then, the feed flow containing 50% CO_2 and 50% N_2 was introduced to the system. It is worth noting that the flowrate and temperature variations were recorded during all adsorption−desorption experiments; also, the compositions were monitored at the outlet flow.

3. ADSORPTION EQUILIBRIUM ISOTHERM AND ISOSTERIC HEAT OF ADSORPTION

A variety of isotherm equations have been employed to fit adsorption equilibrium values.[47] Among them, the dual-site Langmuir model (DSL)[48] has been recognized as a valuable one due to its simplicity, thermodynamic consistency, as well as ability to be easily extended to predict multicomponent sorption equilibria. The isotherm equation is given by eq 1:[48]

$$q_i = q_{m,1}\frac{b_1 P}{1 + b_1 P} + q_{m,2}\frac{b_2 P}{1 + b_2 P} \quad (1)$$

Here, q_m is the saturation adsorbed concentration, P is the equilibrium pressure, and q_i is the adsorbed concentration of the component i. Also, b is the adsorption affinity constant estimated by the Van't Hoff equation:[48,49]

$$b = b^{\infty}\exp\left(-\frac{\Delta H}{RT}\right) \quad (2)$$

https://doi.org/10.1021/acs.iecr.2c04150
Ind. Eng. Chem. Res. 2023, 62, 5216−5229

where $(-\Delta H)$is the heat of adsorption, T the temperature of the system, and R the ideal gas constant. Also, b^{∞}specifies the adsorption affinity constant at infinite temperature. It is worth noting that in model fitting, considered standard deviation between numerical and experimental values is measured by

$$S_D = \sqrt{\frac{1}{N}\sum_{i=1}^{N}(q_i^{exp} - q_i^{cal})^2} \quad (3)$$

The isosteric heat of adsorption (ΔH_{iso}) as a key information related to the energetics of sorption was calculated by the Clausius−Clapeyron equation as[49,50]

$$(-\Delta H_{iso}) = RT^2\left(\frac{\partial \ln p}{\partial T}\right)_{q=constant} \quad (4)$$

By integrating eq 4 at a fixed coverage in a plot of ln p against $1/T$, the isosteric heat can be directly estimated as

$$\ln p = constant - \frac{\Delta H_{iso}}{RT} \quad (5)$$

4. ADSORPTION KINETICS

The sorption kinetics uptake rates of CO_2, CH_4, and N_2 in shaped MIL-160(Al) can be estimated roughly by a solid-film-resistance linear-driving-force model (LDF), which provides a simple mathematical relation to calculate rate coefficients in the piezometric/volumetric sorption system used in this work.[51] The respective lumped K_{LDF} parameters were calculated directly from the sorption uptake experiments in the batch adsorber with a methodology described elsewhere.[46] Briefly, the mass transfer coefficients k_{LDF} for a finite volume variable pressure linear system can be calculated by[46]

$$\frac{C_b}{C_{b0}} = \frac{1}{(K'+1)} + \frac{K'}{(K'+1)}\exp[-(1+K')k_{LDF}t] \quad (6)$$

where C_b is the bulk gas concentration, C_{b0} the initial gas concentration, and k_{LDF} the linear driving force mass transfer coefficient. Also, K' specifies the ratio of the equilibrium sorbate concentration in the solid phase relative to the gas phase represented by $K' = \frac{(m/\rho_p)K}{V}$, where K is the differential slope (or secant of the adsorption equilibrium isotherm) between the initial and final pressure uptake. Now, by defining $\lambda \equiv \frac{C_{b0} - C_{b\infty}}{C_{b0}}$ and considering $K' = \frac{\lambda}{1-\lambda}$, where $C_{b\infty}$ is the final equilibrium concentration, the fractional uptake curve for the batch adsorber system can be represented by[46]

$$F(t) = \frac{C_{b0} - C_b}{C_{b0} - C_\infty} = 1 - \exp[-(1+K')k_{LDF}t] \quad (7)$$

In an infinite volume batch adsorber system, K' is very small, and consequently, eq 7 can be simplified to[52]

$$F(t) = \frac{C_{b0} - C_b}{C_{b0} - C_\infty} = 1 - \exp[-k_{LDF}t] \quad (8)$$

Both eqs 7 and 8 can be applied for a rough estimation of the lumped mass transfer coefficients (k_{LDF}). After that, they can be employed in developing cyclic adsorption processes and the dynamic simulation of continuous fixed-bed adsorption systems.[46,49]

5. SEPARATION PERFORMANCE: SELECTIVITY AND WORKING CAPACITY

The separation potential can be assessed in terms of the adsorption equilibrium selectivity, specified by $S_{i,j} = (q_i/p_i)/(q_j/p_j)$, where q and p are the loading capacities and the equilibrium pressure of sorbates, respectively.[53] The working capacity (β_p) is also another useful adsorption separation performance parameter, which is defined as the difference between the adsorption loading capacities at the high and low pressures in the case of PSA/VSA or at the high and low temperatures for the TSA process. A general approach for working capacity is defined by $\beta_P = q(T_1, p_1) - q(T_2, p_2)$, where q is the adsorption loading capacity at the specified operating conditions of each adsorption step.[54]

6. STATISTICAL ANALYSIS

The statistical analysis of adsorption equilibrium data is also performed using the RSM, which is a topology that combines the statistical and mathematical operations for pattern recognition, designing the experiments, specifying the interactions, and determining optimum values for selected specific data.[55,56] As an example, it can be used to predict easily the best selectivity for separating mixtures as a function of temperature and pressure using measured adsorption equilibrium data. Accordingly, the independent variables, which characterize the system, are considered as factors of methodology, and the dependent variables are evaluated as response surfaces.[57,58] Afterward, the analysis of variance (ANOVA) of the developed surfaces is accomplished regarding the considered factors. In this study, the Historical Data tool of the Design Experts software v.8.0 was employed. The temperature and pressure were considered as factors for analysis of the adsorption process, with the adsorption equilibrium and selectivity being defined as response surfaces. In this way, the statistical analysis of developed adsorption equilibrium values is accomplished using a quadratic polynomial function as

$$y = \beta_0 + \beta_1 x_1 + \beta_2 x_2 + \beta_{12} x_1 x_2 + \beta_{11} x_1^2 + \beta_{22} x_2^2 + \varepsilon \quad (9)$$

here, $y$is the dependent variable (the response surface), and $x_1$and x_2 indicate the considered factors, which are specified in three different levels (−1, 0, and +1).[1,55] Also, β_1 and β_2 illustrate the linear coefficients; β_{12} is a constant, which specifies the interaction among the independent variables; and β_{11} and β_{22} are the quadratic coefficients of the developed model. Furthermore, β_0 and ε are the intercept parameter and the residual error, respectively.[56,57] Then, the defined coefficients are calculated by applying multiple regression analysis and the least square method to develop a significant model by considering the probability of the coefficients (p value), also representing a nonsignificant lack-of-fit.[56] In the end, the precision of the obtained approach is tested in terms of the standard deviation (eq 10) and the regression coefficients (R^2 and adjusted R^2; eqs 11 and 12, respectively):[55,57]

$$\text{Std. dev.} = \sqrt{\frac{\sum_{i=1}^{n}(y_i - \hat{y}_i)^2}{n - P}} \quad (10)$$

https://doi.org/10.1021/acs.iecr.2c04150
Ind. Eng. Chem. Res. 2023, 62, 5216−5229

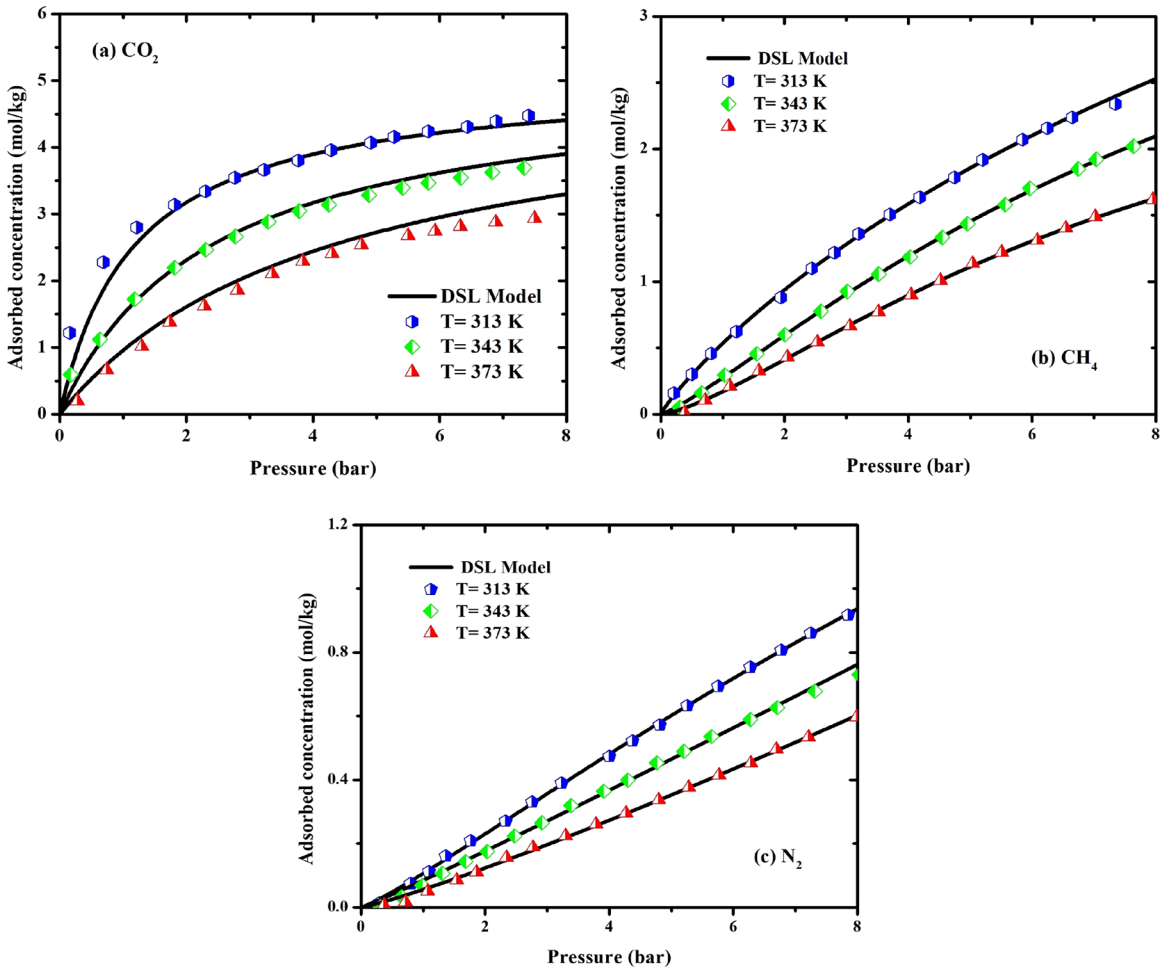

Figure 1. Adsorption equilibrium isotherms of (a) CO_2, (b) CH_4, and (c) N_2 on shaped MIL-160(Al) at 313, 343, and 373 K.

Table 5. . Fitting Parameters of the DSL Model for CO_2, CH_4, and N_2 Adsorption Equilibrium onto Shaped MIL-160(Al)

	q (mol/kg)		$(-\Delta H)$ (kJ mol^{-1})		b^{∞} (bar^{-1})		
species	$q_{m,1}$	$q_{m,2}$	$(-\Delta H)_1$	$(-\Delta H)_2$	$(b^{\infty})_1$	$(b^{\infty})_2$	S_D
CO_2	4.51	5.12	31.5	21.1	3×10^{-4}	2.7×10^{-4}	0.01
CH_4	5.25	1.29	12.1	5.2	6.5×10^{-4}	0.019	0.005
N_2	3.35	2.18	7.21	4.5	2.1×10^{-4}	2.3×10^{-4}	0.008

$$R^2 = 1 - \frac{\sum_{i=1}^{n}(y_i - \hat{y}_i)^2}{\sum_{i=1}^{n}(y_i - \bar{y})^2} \quad (11)$$

$$\text{Adj-}R^2 = 1 - \frac{(1 - R^2)(n - 1)}{(n - P - 1)} \quad (12)$$

Here, $P$is the number of predictors, and n is the number of experiments. Also, $\hat{y}_i$and y_i are the estimated data and experimental results, respectively.[55,57]

7. FIXED-BED ADSORPTION BREAKTHROUGH MODELING

The modeling of fixed-bed breakthrough concentration profiles is fundamental to understand the dynamics of adsorption columns for a proper design of cyclic adsorption processes. Accordingly, a fixed-bed adsorption model was developed to predict/simulate fixed-bed adsorption experiments. The set of governing equations is reported in Table S4 (Supporting Information). The following assumptions were also made:

- The gas phase is described by the ideal gas law.
- The LDF model is employed for mass transfer estimation.
- Each component represents a constant heat of adsorption
- The enthalpy of adsorbed phase is negligible in the solid-phase energy balance.
- The pressure drop is calculated by the Ergun equation.
- Mass and thermal axial dispersion is considered in the column (radial ones are neglected).

The obtained set of partial differential/algebraic relations was numerically solved by Aspen Adsim V-9, employing the method of lines to solve the resulting time-dependent differential/algebraic equations.[59] Also, the flux limiter with van Leer was applied to discretize the spatial coordinate derivatives. More details regarding the auxiliary relations for

https://doi.org/10.1021/acs.iecr.2c04150
Ind. Eng. Chem. Res. 2023, 62, 5216−5229

estimating the parameters of the mathematical model can be found in Table S4 (Supporting Information).

8. RESULTS AND DISCUSSION

8.1. Adsorption Equilibrium Isotherms. The adsorption of CO_2, CH_4, and N_2 on the shaped MIL-160(Al) was studied at 313, 343, and 373 K from vacuum pressure until 8 bar using the piezometric/volumetric technique described previously. The measured adsorption equilibrium values of CO_2, CH_4, and N_2 are illustrated in Figure 1. Also, the experimental numerical values of all isotherms are reported in the Tables S1−S3 (Supporting Information). As mentioned, the DSL model was considered to fit the obtained data, and the fitting parameters are reported in Table 5. Over the entire range of temperatures and pressures studied, the isotherm model fits the experimental results accurately. The amount adsorbed of CO_2 in the shaped MIL-160(Al) is significantly higher than the one in CH_4 and N_2 following the hierarchical order $CO_2 > CH_4 > N_2$ (e.g., 2.8, 0.63, and 0.14 mol/kg at 313 K and 1.2 bar, respectively, for CO_2, CH_4, and N_2). Also, as can be observed, in all studied sorbates (Figure 1), when the temperature increases, the loading capacity decreases, which means that the data follow a normal trend. Moreover, at the lower temperature isotherms, the pressure increment has more impact on the adsorption capacity. Overall, the modeling results described by the lines in Figure 1 demonstrate that the DSL isotherm seems to be reasonable to correlate the observed adsorption equilibrium data for all adsorbable species.

8.2. Isosteric Heat of Adsorption. The isosteric heat of adsorption of CO_2, CH_4, and N_2 as a function of the experimental measured amount adsorbed was calculated using the Clausius−Clapeyron equation (eq 5), and the results are illustrated in Figure 2. As shown, CO_2 and N_2 have the highest

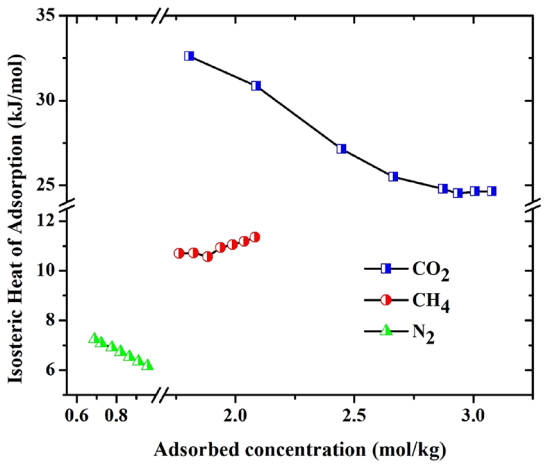

Figure 2. Isosteric heats of adsorption on shaped MIL-160(Al) for CO_2, CH_4, and N_2 as a function of the adsorbed amount at 313−373 K.

and lowest heat of adsorption, respectively. Concerning CO_2, at the low loading of 1 mol/kg, the value is −32 kJ/mol, showing a decreasing trend to around −25 kJ/mol at around 3 mol/kg. For CH_4, an almost constant heat of −11 kJ/mol was observed as a function of the adsorbed amount. Regarding N_2, the value is practically around −7 kJ/mol with a small linear decreasing trend with increasing adsorbed amount. It should be noted that these observed values are different from the ones already shown by Borges et al.[60] for CO_2, CH_4, and N_2 measured in powdered material and predicted by CBMC, where for CO_2, it ranged from −27 to −32 kJ/mol with a slight increasing trend, being −19 kJ/mol for CH_4 and −15 kJ/mol for N_2 and almost constant with increasing loading. A possible explanation is the fact that this work was performed in shaped MOFs which are known to impact the sorbent−sorbate interactions due to the manufacturing procedure. However, note that the range of temperatures studied in both studies is completely different: between 313 and 373 K here against 293 to 313 K in the work of Borges et al.[60] The comparison with other MOFs has been clearly addressed in the work by Borges et al.,[60] where, generally, the heat of adsorption of CO_2 observed in MIL-160(Al) is lower, which can favor its easier regeneration in cyclic operation. Apart from being different in this work, the trends of the isosteric heats are in a certain way similar.

8.3. Adsorption Kinetics. As discussed in Section 4, Karimi et al[46] recently developed a simple kinetic model for directly assessing lumped mass transfer coefficients (K_{LDF}) from the uptake rate data measured in constant-volume variable-pressure batch adsorbers (a finite system). The lumped mass transfer coefficients (k_{LDF}) can be calculated directly from the batch adsorber model described by eq 7. It is worth noting that because of the fast fractional uptake rates of N_2 during the adsorption equilibrium studies, they are almost unreliable to measure. Thus, here, only LDF coefficients of CO_2 and CH_4 onto shaped MIL-160(Al) are reported, where uptake rates measured are reliable over small pressure steps, to eliminate as much as possible the effect of nonlinearities of the isotherm and also heat effects (in accordance with the model described by eq 7) which is only achieved near the low-pressure range of the respective isotherms measured. Accordingly, the LDF values calculated are in the order of 0.021−0.096 and 0.041−0.165 s^{-1} at 313 K between 0.11 and 2.76 bar for CO_2 and CH_4, respectively. Tables S5 and S6 (Supporting Information) specify the calculated mass transfer coefficients (k_{LDF}) for CO_2 and CH_4, respectively, around the respective pressure range measured; also, Figures 3 and 4 elucidate some of the fractional uptake rate fitting curves with eq 7.

As can be observed, there is a satisfactory agreement between modeling values and experimental results. For instance, Figure 3a (uptake rate data of CO_2 at 313 K) shows that at the final equilibrium pressure of 0.109 bar, the uptake to equilibrium takes around 80 s, whereas at the higher pressure (2.301 bar), it requires approximately 35 s. The same trends can be observed at 373 K (after around 25 s) (Figure 3c). Also, Figure 4 shows the uptake rates of CH_4, which are higher than those of CO_2 at the same operating conditions. The derived k_{LDF} values are reported in Tables S5 and S6. As can be found, in all studied isotherms, as expected, the faster uptake rates are observed as the pressure rises. For example, the k_{LDF} of CO_2 at 313 K demonstrates that at the pressures around 0.11 and 2.76 bar, the values increase from 0.021 to 0.096 s^{-1}; also, a similar behavior can be observed by increasing the temperature, in which the highest k_{LDF} value is obtained at 2.8 bar and 373 K: 0.584 s^{-1}. Similarly, the k_{LDF} values of CH_4 increase by increasing the temperature and pressure (Table S6); but in this case, the uptake rates are faster than those of CO_2. These values are in the same range as the one observed by Streb and Mazzotti[51] on the large-pore zeolite 13X and are also in line with a fast mass transfer for the shaped MIL-160(Al).

https://doi.org/10.1021/acs.iecr.2c04150
Ind. Eng. Chem. Res. 2023, 62, 5216−5229

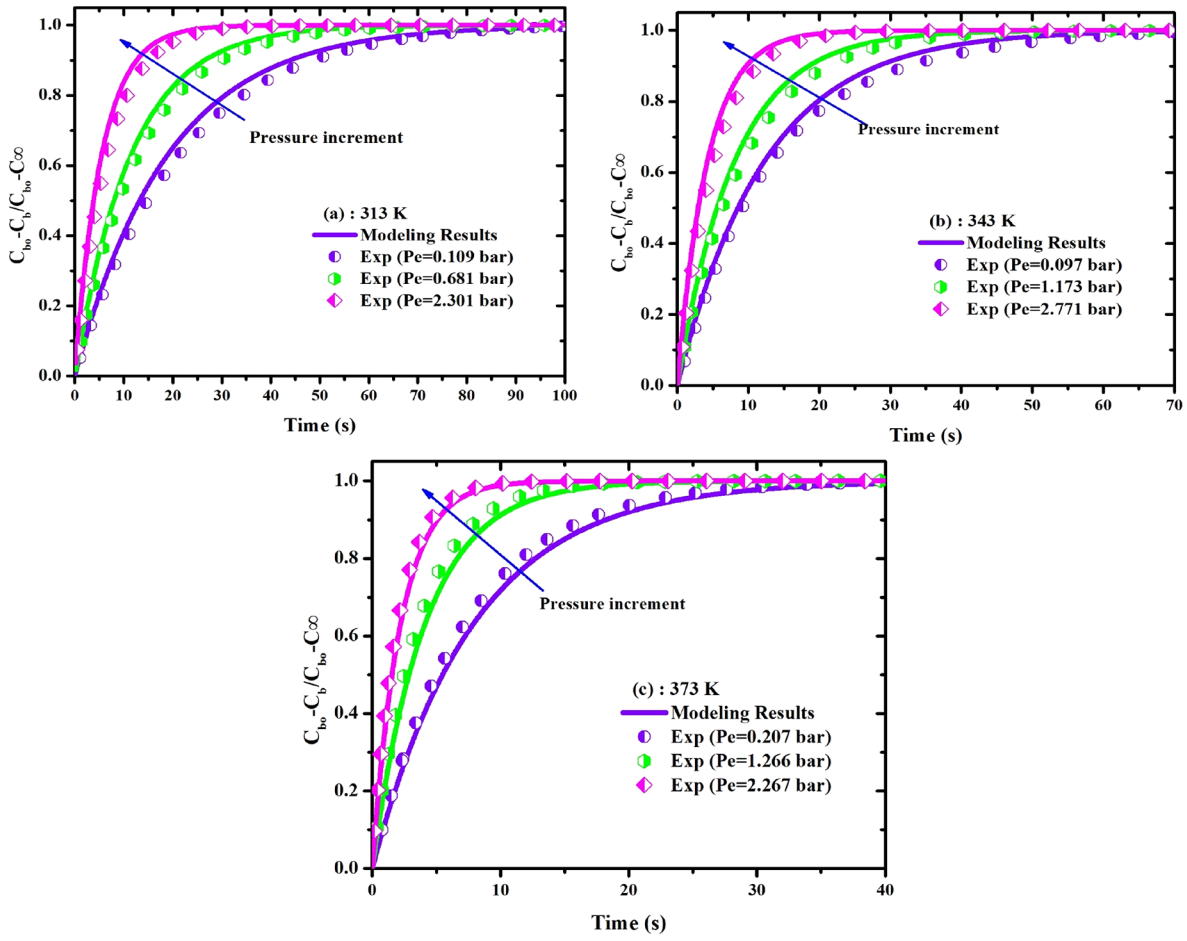

Figure 3. Selected experimental uptake rates of CO_2 and fitting values with the batch adsorber model (eq 6) at (a) 313 K, (b) 343 K, and (c) 373 K.

Further, a plausible explanation to elucidate the pressure dependency of the k_{LDF} with increasing loading can be related to the decreasing slope of the isotherm.[49] The enhancement of k_{LDF} parameters with temperature is expected because as temperature increases, kinetic mechanisms are faster because it is an activated phenomenon.[61] A comparison between the values of k_{LDF} in MIL-160(Al) and some benchmark zeolites or other sorbents for CO_2 adsorption is reported in Table 6. One can observe that the values reported here are similar to the ones observed for zeolite 13X, which means fast kinetics. Note also that in most MOF sorption studies performed, such kinetic data regarding the calculation of k_{LDF} values are not available because it involved powdered material. Accordingly, a direct comparison with other MOFs is practically impossible unless further studies using shaped MOFs are performed, which is not yet the case to the best of our knowledge.

8.4. Selectivity and Working Capacity. Based on the single component equilibrium data, the calculated selectivities (50/50, v/v) at 313 and 343 K are illustrated in Figure 5. As shown, the selectivity for the binary system CO_2/N_2 is higher than that for CO_2/CH_4. For instance, for CO_2/N_2 and CO_2/CH_4 at 313 K and 1.5 bar, the values are 18 and 4, respectively. Also, the isotherms of CO_2 in MIL-160(Al) are not so favorable as the ones in zeolite 13X,[51] which favor the desorption/regeneration step in cyclic operations with also a higher working capacity. Accordingly, if one correlates these values to the fast kinetics, shaped form, and excellent thermal stability of MIL-160(Al), this shows the potential of this adsorbent for the development of cyclic adsorption processes concerning CCS (e.g., postcombustion) or BU.[62]

The working capacity for a TSA process at 1.2 bar calculated in the temperature range of 313−343 K is around 1.07 mol kg^{-1}, whereas in a temperature range of 313−373 K, the same pressure becomes 1.85 mol kg^{-1}. Furthermore, the calculated working capacity for a PSA process at 313 K and pressure range between 0.5 and 7 bar is around 2.38 mol kg^{-1}, whereas at 343 K, it is a little bit smaller at 2.15 mol kg^{-1}, which can be compared with ones already reported at 298 K at the same pressure range: Mg-MOF-74: 2.1 mol kg^{-1}, zeolite 13X: 1.75 mol kg^{-1}, and UTSA-16: 1.44 mol kg^{-1}.[63] These results show that MIL-160(Al) can be regarded as an important sorbent for CCS and BU using TSA or PSA processes. However, an accurate grasp regarding the large-scale applications requires further comprehensive experimental works; nonetheless, the results from this work are very promising.

8.5. Statistical Analysis. *8.5.1. Adsorption Equilibrium Results.* The Historical Data tool of RSM was considered for the statistical analysis of the adsorption equilibrium values of CO_2, CH_4, and N_2 onto shaped MOF MIL-160(Al). Accordingly, the obtained equilibrium results from the volumetric unit were introduced as input factors of quadratic polynomial functions in the RSM according to the procedure described in Section 6. Also, a detailed description of the statistical analysis of adsorption equilibrium results is presented

https://doi.org/10.1021/acs.iecr.2c04150
Ind. Eng. Chem. Res. 2023, 62, 5216−5229

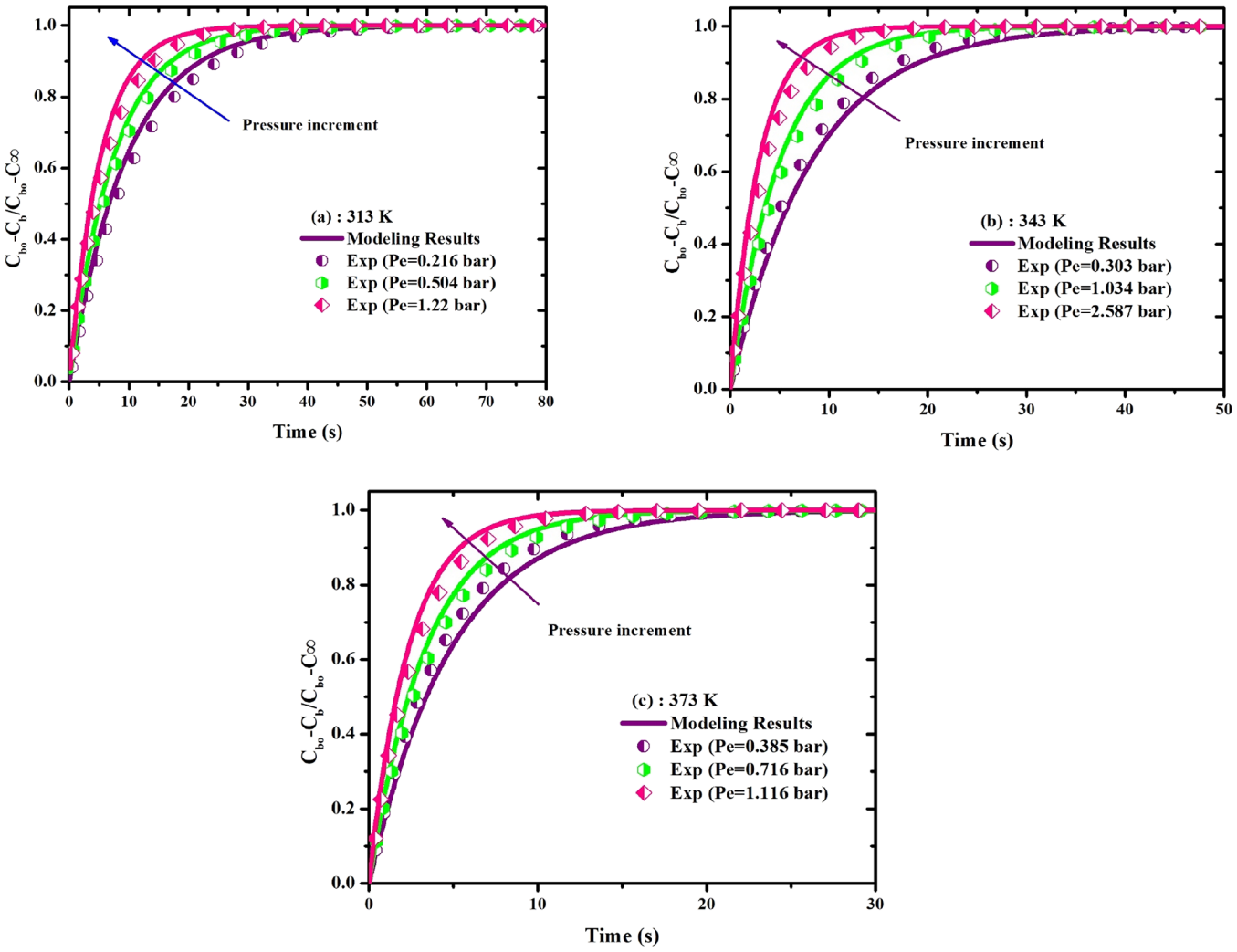

Figure 4. Selected experimental uptake rates of CH_4 and fitting values with the batch adsorber model (eq 6) at (a) 313 K, (b) 343 K, and (c) 373 K.

Table 6. A Comparison between CO_2 K_{LDF} Mass Transfer Coefficients in Shaped MIL-160(Al) and Other Reference Sorbents

sorbents	temperature (K)	K_{LDF} (s^{-1})	ref
zeolite 13X	298	0.06	51
binderless zeolite 4A	303	0.08	46
honeycomb carbon monoliths	303	0.025	70
silica gel	303	0.064	71
zeolite CaX	313	0.013	72
zeolite MgX	313	0.071	72
MIL-160(Al)	313	0.052	this work

in Appendix A (Supporting Information). The response surfaces of obtained models have been plotted in Figure S2 (Supporting Information). As can be expected, there is an excellent accordance regarding the adsorption concepts and developed surfaces, which proves the reliability of the data collected. As illustrated and expected, in all represented plots (Figure S2a–c), the pressure increment contributes to the loading enhancement, whereas the temperature represents a negative effect on the adsorption capacity.[48,49] In addition, at the lower temperatures, the pressure increase demonstrates a significant impact on the equilibrium adsorption than the higher temperatures, which this behavior can clearly be found in (Figure S2a).

8.5.2. Separation Performance: Selectivity and Working Capacity. Taking into account the reliability of the RSM methodology to analyze the adsorption equilibrium data, this method was also applied to find the combination of the best operating conditions (temperature and pressure) to improve the selectivity CO_2/CH_4 and CO_2/N_2 in MIL-160(Al) in view of designing cyclic adsorption processes for BU and CCS. To this end, first, the selectivity of each process as a response surface was analyzed to derive the significant topologies in the studied operating conditions: T = 313−373 K and P = 0.1−7 bar. Accordingly, response surface plots are depicted in Figure 6 (detailed information about the numerical procedure can be found in the Supporting Information); also, the derived ANOVA results are reported in Table S8s (Supporting Information). As can be observed, the proposed models are significant with admissible results for R^2, Adj-R^2, Pred-R^2, and standard deviation (the justifications of parameters have been discussed in the Supporting Information). Afterward, an optimization approach was applied by employing 30 iterations per model to determine the optimum values for selectivities of CO_2/N_2 and CO_2/CH_4 for developing cyclic adsorption processes for BU and CCS (e.g., postcombustion processes).

https://doi.org/10.1021/acs.iecr.2c04150
Ind. Eng. Chem. Res. 2023, 62, 5216−5229

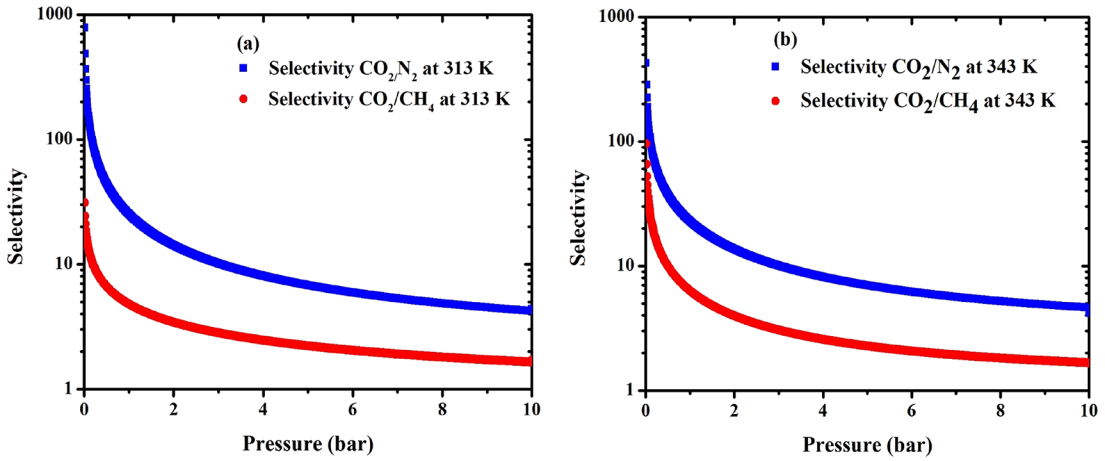

Figure 5. A comparison on different selectivities onto shaped MIL-160(Al) at (a) 313 K and (b) 343 K.

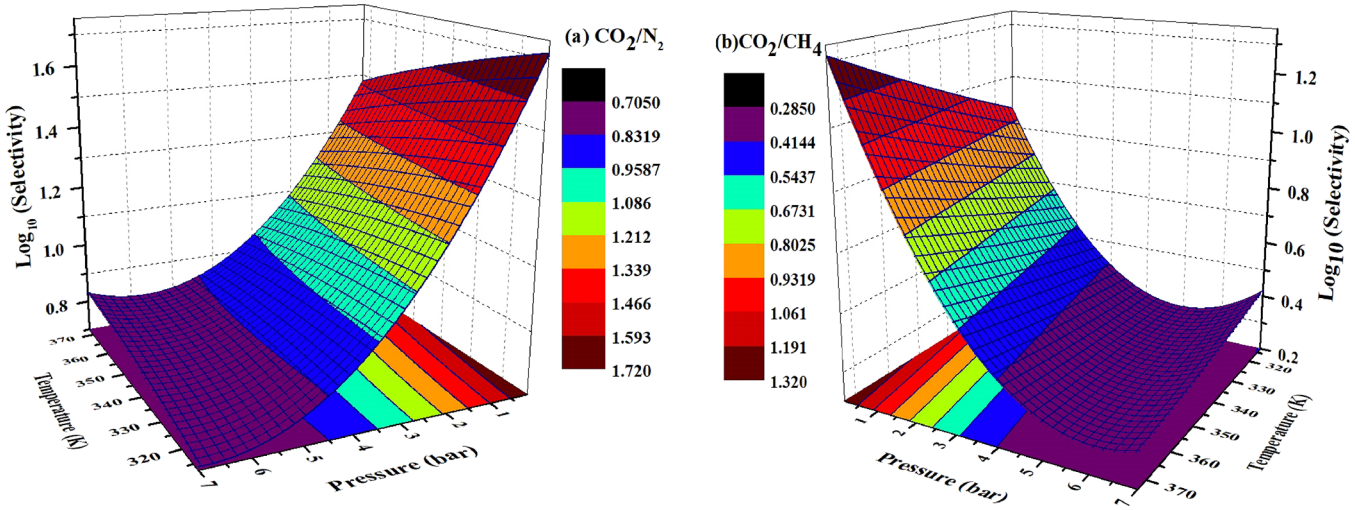

Figure 6. Response surface plots of selectivities onto shaped MIL-160(Al) for (a) CO_2/N_2 and (b) CO_2/CH_4 at studied temperatures and pressures.

The results given by the RSM methodology specified the best value of 9.75 for the selectivity of CO_2/N_2, which corresponds with T = 313 K and P = 3.14 bar, and 2.59 for the selectivity of CO_2/CH_4, which is related with T = 313 K and P = 3.57 bar. These operating conditions were therefore employed to evaluate the dynamics of fixed-bed adsorption for the binary separations of CO_2/CH_4 and CO_2/N_2 on MIL-160(Al) in a fixed-bed adsorber.

8.6. Multicomponent Dynamic Adsorption of CO_2/CH_4 and CO_2/N_2 on MIL-160(Al) in a Fixed-Bed Adsorber. To prove the reliability of the measured adsorption equilibrium and kinetic results and access information about the dynamics of fixed-bed adsorption, two breakthrough experiments were accomplished. Accordingly, in our case, the dynamics of fixed-bed adsorption of a binary mixture of CO_2/CH_4 (50−50%) and a pseudobinary of CO_2/N_2 (50−50%) were evaluated by measuring the respective breakthrough curves at the total pressure of 3 bar and temperature of 313 K. Details regarding the breakthrough experimental unit and operating conditions can be found in Table 4. Figures 7 and 8 illustrate the breakthrough experiments for the binary systems CO_2/CH_4 and CO_2/N_2, respectively, together with prediction/modeling results and temperature history during both the adsorption−desorption steps. The numerical model details of the simulations are described in Table S4 (Supporting Information). It is noteworthy that in the simulation of the breakthrough experiments using ASPEN Adsorption (lines in Figures 7 and 8), the adsorption equilibrium data and the K_{LDF} parameters (eq E.S.4 in Table S4) are the ones presented in the previous sections, and particularly for N_2, we found that K_{LDF} values higher than the ones measured for CO_2 and CH_4 do not influence the shape of the N_2 breakthrough profiles. In addition, the axial dispersion in the fixed-bed column was estimated using the Langer et al. correlation (eq E.S.12 in Table S4).[49] As observed in Figures 7 and 8, the theoretical predictions reasonably match the experiments, which prove the reliability of all the data measured through this work taken from independent experiments (adsorption equilibrium and kinetic data). The general overview of the breakthrough curve of CO_2/CH_4 shown in Figure 7a demonstrates the typical roll-up effect in which the CH_4 molar flowrate practically doubles the inlet molar flowrate, indicating a strong displacement of the adsorbed CH_4 by CO_2 due to the adsorption equilibrium competition (NB: the extended DSL model was used to predict the multicomponent sorption equilibria in ASPEN Adsim simulations). Furthermore, the kinematic traveling waves have sharp molar flowrate fronts especially for CH_4 that are expected from the relatively high K_{LDF} coefficients

https://doi.org/10.1021/acs.iecr.2c04150
Ind. Eng. Chem. Res. 2023, 62, 5216−5229

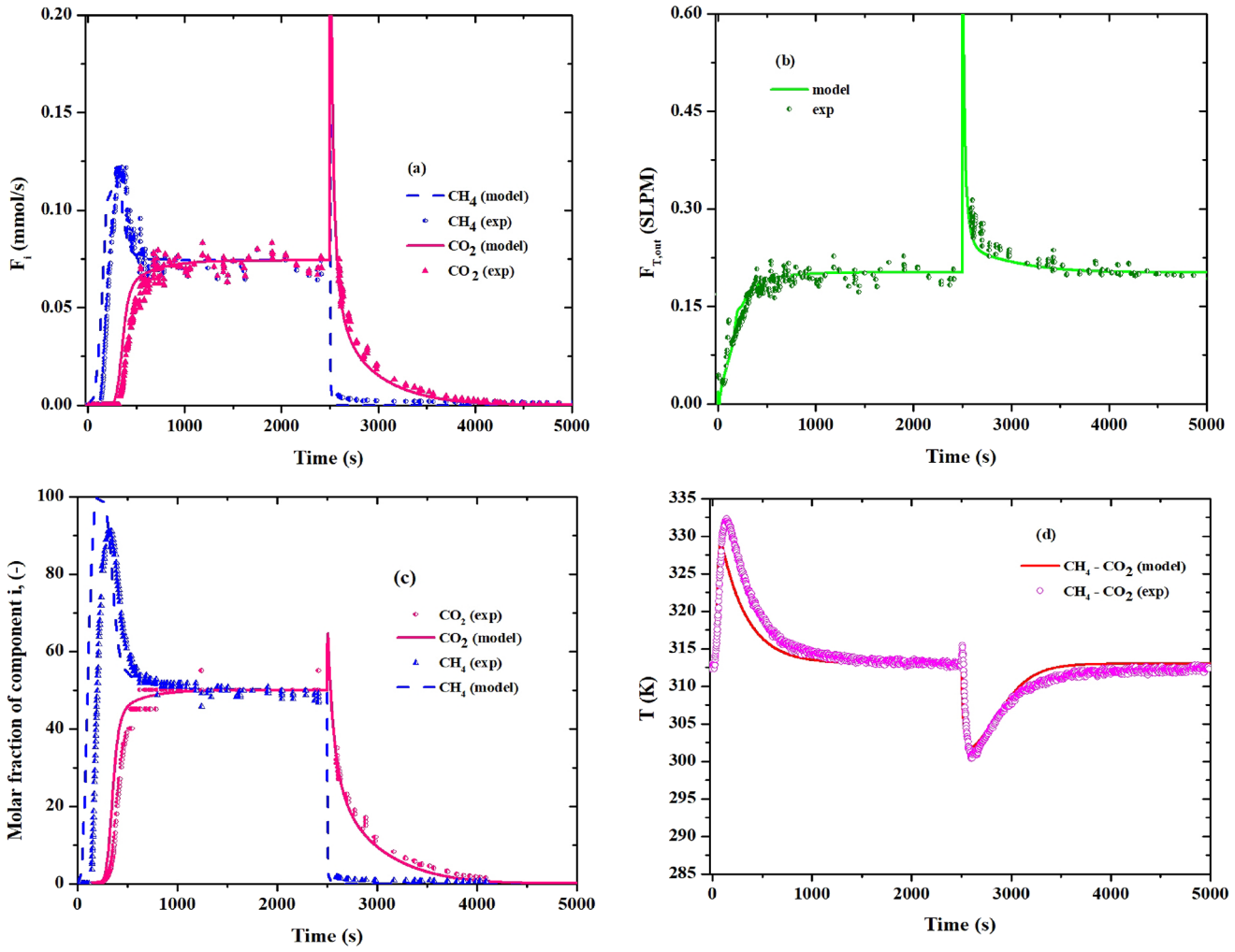

Figure 7. Fixed-bed breakthrough dynamic adsorption−desorption binary experiment of CO_2/CH_4 (50%−50%) at 313 K and 3 bar. (a) Molar flowrate of CO_2 and CH_4 at the binary mixture, (b) total flow rate, (c) molar fraction, and (d) temperature history. Symbols are experimental data, and lines are model predictions. Experimental conditions and model parameters are provided in Table 4 and Table S4.

measured in the batch experiments. In Figure 8, the potential of MIL-160(Al) for CO_2/N_2 separation concerning CCS has also been evaluated, in which the bed was first saturated with pure N_2 and fed with a flow containing CO_2/N_2 (50−50%). Once more, an acceptable agreement between the experimental results (indicated by symbols) and simulation values (indicated by lines) can be observed, proving that the developed model is reliable for understanding the fixed-bed adsorption dynamics. The outlet temperature histories of CO_2/CH_4 and CO_2/N_2 are presented in Figures 7d and 8d, respectively, which show the correspondent temperature increase of CO_2/CH_4 and CO_2/N_2 in the bed during the adsorption step (exothermic process) to the values around 20 and 15 K, respectively, and the corresponding reverse in the desorption step (endothermic process) by the same values during the passage of the mass transfer zone in such locations of the bed. The modeling results also predict satisfactorily the temperature histories in the bed. Generally, the regeneration of the bed is easily made because of the fast kinetics of CO_2, CH_4, and N_2 and also the isotherm shape of CO_2, which is not so favorable, for example, as in zeolite 13X,[51] which favors the cleaning of the bed in the desorption. It is worth noting that the desorption of the CO_2/CH_4 breakthrough experiment was accomplished by passing the pure methane in the column, whereas in the CO_2/N_2 experiment, it was performed using pure nitrogen.

8.7. Comparison with Other Sorbents. The sorption properties of MIL-160(Al) for BU and CCS studied in this work such as selectivity, loading capacity, isosteric heat of adsorption, and surface area have been compared in Table S9 (Supporting Information) with other relevant sorbents. For instance, MIL-101(Cr),[33,64] amine-MIL-101(Cr),[65] UiO-66[66] and CuBTC[67−69] exhibit CO_2 loading capacities (mmol/g) of 1.55, 1.9, 1.55, and 1.65 at 1 bar and 313 K, respectively, compared with 2.75 (mmol/g) for MIL-160(Al) at the same operating conditions. Further, MIL-101(Cr),[33,64] besides a higher heat of adsorption (CO_2: 44, CH_4: 18, and N_2:19.66 kJ/mol), also presents a lower selectivity concerning the CO_2/CH_4 and CO_2/N_2 separations. Thus, MIL-160(Al), due to its unique features such as stability, cost, and easy shaping,[42,44,45] appears as a very competitive sorbent for large-scale applications of CO_2 separation under BU and CCS strategies, among others.[41,44]

9. CONCLUSIONS

The adsorption equilibrium of CO_2, CH_4, and N_2 into the shaped microporous Al carboxylate MIL-160(Al) was evaluated using a piezometric/volumetric technique from

https://doi.org/10.1021/acs.iecr.2c04150
Ind. Eng. Chem. Res. 2023, 62, 5216−5229

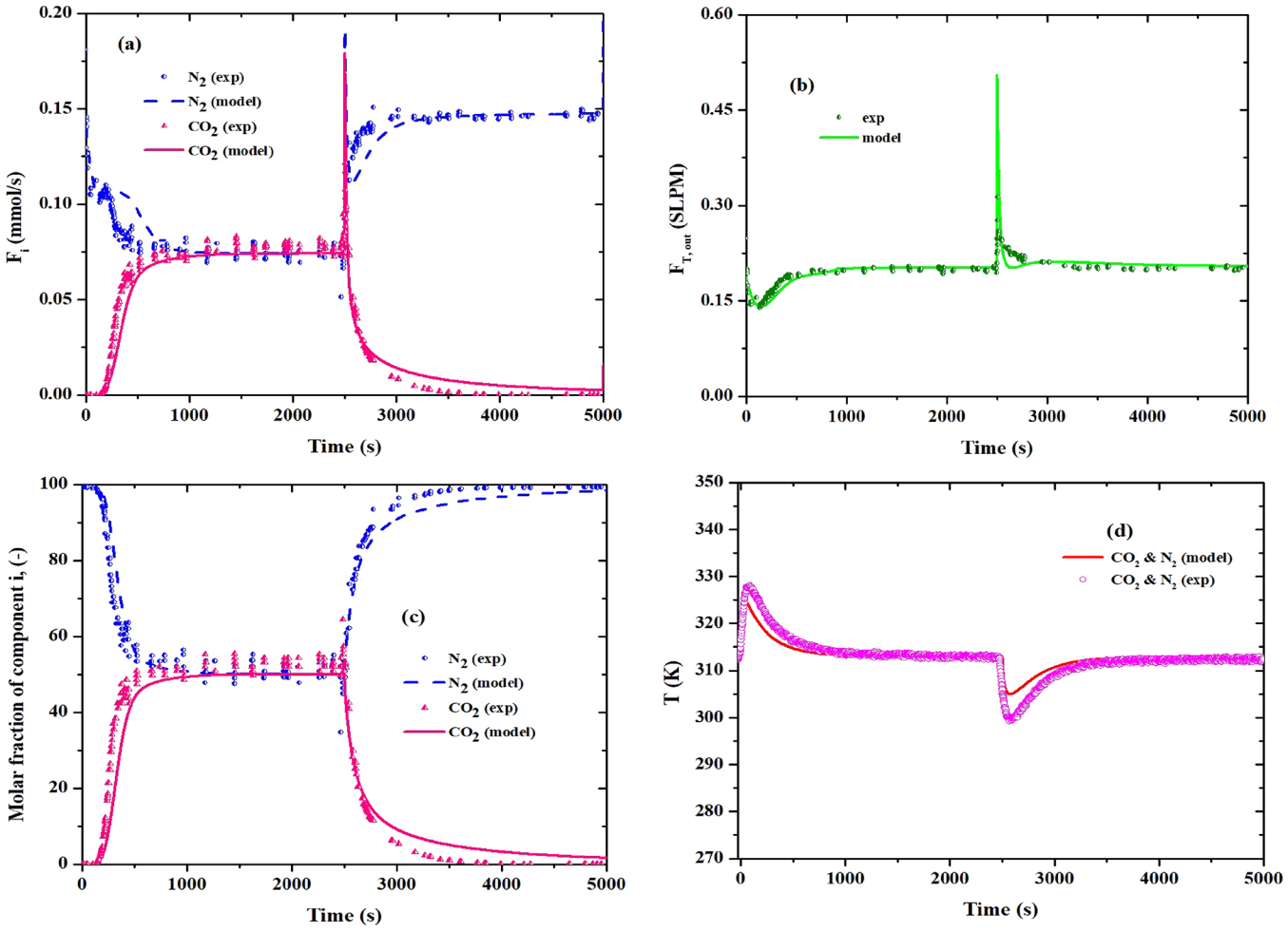

Figure 8. Fixed-bed breakthrough dynamic adsorption−desorption pseudobinary experiment of CO_2/N_2 (50%−50%) at 313 K and 3 bar. (a) Molar flowrate of CO_2 and N_2 at the pseudobinary mixture, (b) total flowrate, (c) molar fraction, and (d) temperature history. The bed was initially full of nitrogen. Symbols are experimental data, and lines are model predictions. Experimental conditions and model parameters are provided in Table 4 and Table S4.

subatmospheric pressure until 8 bar at 313, 343, and 373 K under relevant BU and CCS (postcombustion) operating condition processes. The dual-site Langmuir (DSL) isotherm was employed to describe the measured experimental isotherms, showing that CO_2 has the highest affinity (e.g., 3.8, 1.5, and 0.44 mol/kg for CO_2, CH_4, and N_2, at 3.7 bar and 313 K, respectively). The single component adsorption selectivities for CO_2/N_2 and CO_2/CH_4 are around 18 and 4 at 1.5 bar and 313 K, respectively. The working capacity taken from the adsorption equilibrium data for a PSA process at 313 K in the pressure range 0.159−7.404 bar was around 3.26 mol kg^{-1}. The kinetics of sorption studied from uptake rate experiments using a solid-film linear-driving-force model (LDF) is in the range of 0.021−0.096 s^{-1} at 313 K and 0.11−2.76 bar for CO_2, and for CH_4, it was in the range of 0.041−0.165 s^{-1} at 313 K and 0.216−2.44 bar, which can be considered as a high mass transfer rate by comparing with the benchmark large-pore zeolite 13X. The RSM data revealed a value of 9.75 for the selectivity of CO_2/N_2, which corresponds with T = 313 K and P = 3.14 bar, and 2.59 for the selectivity of CO_2/CH_4, which is related with T = 313 K and P = 3.57 bar. Finally, the dynamics of fixed-bed adsorption of binary equimolar mixtures of CO_2/CH_4 and CO_2/N_2 was studied through the breakthrough experiments from where a mathematical model was calibrated taking into account the measured adsorption equilibrium and kinetic data from this work and correlations available in the literature (e.g., estimations of axial dispersion in the bed). The close agreement between simulations and experimental data using ASPEN Adsim proves the reliability of the adsorption equilibrium and kinetic data measured through this work, with the mathematical model being a valuable tool for the design of cyclic adsorption processes (PSA or TSA) to use MOF MIL-160 (Al) in strategies of BU and CCS (postcombustion CO_2 capture) regarding its unique characters including stability, cost, and easy shaping as well as adsorption performance compared with other candidates.

■ ASSOCIATED CONTENT

Supporting Information

The Supporting Information is available free of charge at https://pubs.acs.org/doi/10.1021/acs.iecr.2c04150.

N_2 adsorption−desorption isotherm at 77 K; Tables S1−S3: adsorption experimental values of CO_2, CH_4, and N_2 onto shaped MIL-160(Al), respectively; Table S4: the considered set of equations for simulation of fixed-bed adsorption equilibrium; Tables S5 and 6: mass transfer parameters of CO_2 and CH4 on shaped MIL-

https://doi.org/10.1021/acs.iecr.2c04150
Ind. Eng. Chem. Res. 2023, 62, 5216−5229

160(Al), respectively; Appendix A: detailed description of statistical analysis of adsorption equilibrium results; Table S7: ANOVA results for CO_2, CH_4, and N_2 adsorption assessment; Figure S2: response surface plots of CO_2, CH_4, and N_2; Table S8: ANOVA results for selectivities of shaped MIL-160(Al) for CO_2/N_2 and CO_2/CH_4 at studied temperatures and pressures; and Table S9: separation properties of some recently developed sorbents for BU and CCS capture processes (PDF)

AUTHOR INFORMATION

Corresponding Authors

Mohsen Karimi − *Laboratory of Separation and Reaction Engineering (LSRE), Associate Laboratory LSRE/LCM, Faculty of Engineering and ALiCE-Associate Laboratory in Chemical Engineering, Faculty of Engineering, University of Porto, Porto 4200-465, Portugal; Centro de Investigação de Montanha (CIMO), Instituto Politécnico de Bragança, Campus de Santa Apolónia, Bragança 5300-253, Portugal;* orcid.org/0000-0002-1886-5454; Phone: +351 934 070 714; Email: mohsen.karimi@fe.up.pt

Alexandre Ferreira − *Laboratory of Separation and Reaction Engineering (LSRE), Associate Laboratory LSRE/LCM, Faculty of Engineering and ALiCE-Associate Laboratory in Chemical Engineering, Faculty of Engineering, University of Porto, Porto 4200-465, Portugal;* orcid.org/0000-0002-6746-8973; Phone: +351 22 5084835; Email: aferreir@fe.up.pt

Christian Serre − *Institut des Matériaux Poreux de Paris (IMAP), Ecole Normale Supérieure de Paris, ESPCI Paris, CNRS, PSL University, Paris 75005, France;* orcid.org/0000-0003-3040-2564; Phone: +33 1 44 32 24 63; Email: christian.serre@ens.fr

José A. C. Silva − *Centro de Investigação de Montanha (CIMO), Instituto Politécnico de Bragança, Campus de Santa Apolónia, Bragança 5300-253, Portugal;* orcid.org/0000-0003-1778-3833; Phone: +351 273 30 3125; Email: jsilva@ipb.pt

Authors

Alírio E. Rodrigues − *Laboratory of Separation and Reaction Engineering (LSRE), Associate Laboratory LSRE/LCM, Faculty of Engineering and ALiCE-Associate Laboratory in Chemical Engineering, Faculty of Engineering, University of Porto, Porto 4200-465, Portugal;* orcid.org/0000-0002-0715-4761

Farid Nouar − *Institut des Matériaux Poreux de Paris (IMAP), Ecole Normale Supérieure de Paris, ESPCI Paris, CNRS, PSL University, Paris 75005, France*

Complete contact information is available at: https://pubs.acs.org/10.1021/acs.iecr.2c04150

Notes

The authors declare no competing financial interest.

ACKNOWLEDGMENTS

This work was financially supported by LA/P/0045/2020 (ALiCE), UIDB/50020/2020, and UIDP/50020/2020 (LSRE-LCM), funded by national funds through FCT/MCTES (PIDDAC). Also, it received financial support through national funds FCT/MCTES (PIDDAC) to CIMO (UIDB/00690/2020 and UIDP/00690/2020) and SusTEC (LA/P/0007/2020). Mohsen Karimi also acknowledges the PhD research grant awarded by the Foundation of Science and Technology of Portugal (FCT) under SFRH/BD/140550/2018 project. Authors also acknowledge Kyung-Ho Cho and U-Hwang Lee from Korea Research Institute of Chemical Technology (KRICT), Republic of Korea, for their contributions in the synthesis and shaping MIL-160(Al).

NOMENCLATURE

Symbol	Explanation (Unit)
a	specific particle surface (m^2/m^3)
a_p	specific particle surface per unit volume bed (m^2 (particle area)/m^3 (bed))
A	area (m^2)
C_b	bulk concentration (mol/cm^3)
C_{b0}	initial bulk concentration (mol/cm^3)
c_{ps}	specific heat capacity of adsorbent (MJ/kg/K)
c_{pW}	specific heat capacity of column wall (MJ/kg/K)
c_{vg}	specific gas phase heat capacity at constant volume (MJ/kmol/K)
D_{ax}	axial dispersion coefficient of component k (cm^2/s)
D_B	bed diameter (m)
D_p	pore diffusivity (cm^2/s)
D_k	Knudsen diffusivity (cm^2/s)
D_m	molecular diffusivity (cm^2/s)
D_{rd}	radial dispersion coefficient of component k (cm^2/s)
F_i	molar flowrate of component i (mmol/s)
H_w	gas-wall heat transfer coefficient ($MJ/m^2/s$)
k_{ga}	effective axial gas phase thermal conductivity (MW/m/K)
m	mass of adsorbent in adsorption cell (g)
M	molecular weight (g/mol)
k_{LDF}	linear driving force mass transfer coefficient (1/s)
P	pressure (bar)
P_i	partial pressure of component i (bar)
P_{sat}	saturation pressure (bar)
q	adsorbed amount (mol/kg)
q_m	saturation loading capacity (mol/kg)
r_p	particle radius (cm)
R	universal gas constant (bar m^3/kmol/K)
t	time (s)
T_s	solid-phase temperature (K)
T_g	gas-phase temperature (K)
T_w	wall temperature (K)
V	volume (cm^3)

Greek letters

β_p	working capacity (mol/kg)
ε_B	total bed voidage (m^3 (void + pore)/m^3 (bed))
ε_i	interparticle voidage (m^3 (void)/m^3 (bed))
ε_p	intraparticle voidage (m^3 (pore)/m^3 (bed))
ρ_p	particle density ($kg/m^{3)}$
ρ_g	gas-phase molar density ($kmol/m^{3)}$
ρ_s	adsorbent bulk density (kg/m^3)
ρ_W	wall density (kg/m^3)

Abbreviations

AD	anaerobic digestion
CCS	carbon capture and sequestration
IEA	International Energy Agency
IPPC	Intergovernmental Panel on Climate Change
DSL	dual-site Langmuir
PSA	pressure swing adsorption

https://doi.org/10.1021/acs.iecr.2c04150
Ind. Eng. Chem. Res. 2023, 62, 5216−5229

VSA vacuum swing adsorption
RSM Response Surface Methodology

REFERENCES

(1) Karimi, M.; Silva, J. A. C.; Gonçalves, C. N. D. P.; Diaz De Tuesta, J. L.; Rodrigues, A. E.; Gomes, H. T. CO2 Capture in Chemically and Thermally Modified Activated Carbons Using Breakthrough Measurements: Experimental and Modeling Study. *Ind. Eng. Chem. Res.* **2018**, *57*, 11154−11166.

(2) Bui, M.; Adjiman, C. S.; Bardow, A.; Anthony, E. J.; Boston, A.; Brown, S.; Fennell, P. S.; Fuss, S.; Galindo, A.; Hackett, L. A.; Hallett, J. P.; Herzog, H. J.; Jackson, G.; Kemper, J.; Krevor, S.; Maitland, G. C.; Matuszewski, M.; Metcalfe, I. S.; Petit, C.; Puxty, G.; Reimer, J.; Reiner, D. M.; Rubin, E. S.; Scott, S. A.; Shah, N.; Smit, B.; Trusler, J. P. M.; Webley, P.; Wilcox, J.; Mc Dowell, N. Carbon Capture and Storage (CCS): The Way Forward. *Energy Environ. Sci.* **2018**, *11*, 1062−1176.

(3) Karimi, M.; Rahimpour, M. R.; Rafiei, R.; Jafari, M.; Iranshahi, D.; Shariati, A. Reducing Environmental Problems and Increasing Saving Energy by Proposing New Configuration for Moving Bed Thermally Coupled Reactors. *J. Nat. Gas Sci. Eng.* **2014**, *17*, 136−150.

(4) Shirzad, M.; Karimi, M.; Silva, J. A. C.; Rodrigues, A. E. Moving Bed Reactors: Challenges and Progress of Experimental and Theoretical Studies in a Century of Research. *Ind. Eng. Chem. Res.* **2019**, *58*, 9179−9198.

(5) Karimi, M.; Zafanelli, L. F. A. S.; Almeida, J. P. P.; Ströher, G. R.; Rodrigues, A. E.; Silva, J. A. C. Novel Insights into Activated Carbon Derived from Municipal Solid Waste for CO2Uptake: Synthesis, Adsorption Isotherms and Scale-Up. *J. Environ. Chem. Eng.* **2020**, *8*, No. 104069.

(6) Tangang, F. T.; Juneng, L.; Salimun, E.; Sei, K. M.; Le, J.; Halimatun Muhamad, L. Climate Change and Variability over Malaysia: Gaps in Science and Research Information (Perubahan Dan Keragaman Iklim Di Malaysia: Jurang Dalam Maklumat Sains Dan Penyelidikan). *Sains Malays* **2012**, *41*, 1355−1366.

(7) Ernawati Hamdan, M.; Man, N.; Md Yassin, S.; Lawrence D'Silva, J.; Mohamed Shaffril, H. A. Farmers' Adaptive Capacity towards the Impacts of Global Warming: A Review. *Asian Soc. Sci.* **2013**, *9*, 177.

(8) IPCC. *Climate Change 2022: Impacts, Adaptation and Vulnerability. Contribution of Working Group II to the Sixth Assessment Report of the Intergovernmental Panel on Climate Change*: Cambridge University Press: Cambridge, UK and New York, NY, USA, 3056 *Pp.*; 2022.

(9) IEA. *Energy Technology Perspectives 2010 − Analysis - IEA*. https://www.iea.org/reports/energy-technology-perspectives-2010 (accessed 2021-11-18).

(10) Rubin, E. S.; Tokyo, J. *IPCC Special Report on IPCC Special Report on Carbon Carbon Dioxide Dioxide Capture Capture and and Storage Storage RITE International Workshop on CO 2 Geological Storage*. 2006.

(11) Li, F.; Fan, L. S. Clean Coal Conversion Processes − Progress and Challenges. *Energy Environ. Sci.* **2008**, *1*, 248−267.

(12) Karimi, M.; Aminzadehsarikhanbeglou, E.; Vaferi, B. Robust Intelligent Topology for Estimation of Heat Capacity of Biochar Pyrolysis Residues. *Measurement* **2021**, *183*, No. 109857.

(13) Karimi, M.; Alibak, A. H.; Alizadeh, S. M. S.; Sharif, M.; Vaferi, B. Intelligent Modeling for Considering the Effect of Bio-Source Type and Appearance Shape on the Biomass Heat Capacity. *Measurement* **2022**, *189*, No. 110529.

(14) Naquash, A.; Qyyum, M. A.; Haider, J.; Bokhari, A.; Lim, H.; Lee, M. State-of-the-Art Assessment of Cryogenic Technologies for Biogas Upgrading: Energy, Economic, and Environmental Perspectives. *Renewable Sustainable Energy Rev.* **2022**, *154*, No. 111826.

(15) Scarlat, N.; Dallemand, J. F.; Fahl, F. Biogas: Developments and Perspectives in Europe. *Renewable Energy* **2018**, *129*, 457−472.

(16) Hernández, B.; Martín, M. Optimal Process Operation for Biogas Reforming to Methanol: Effects of Dry Reforming and Biogas Composition. *Ind. Eng. Chem. Res.* **2016**, *55*, 6677−6685.

(17) Kunkel, C.; Vines, F.; Illas, F. Biogas Upgrading by Transition Metal Carbides. *ACS Appl. Energy Mater.* **2018**, *1*, 43−47.

(18) Ferreira, A. F. P.; Ribeiro, A. M.; Kulaç, S.; Rodrigues, A. E. Methane Purification by Adsorptive Processes on MIL-53(Al). *Chem. Eng. Sci.* **2015**, *124*, 79−95.

(19) Ben-Mansour, R.; Habib, M. A.; Bamidele, O. E.; Basha, M.; Qasem, N. A. A.; Peedikakkal, A.; Laoui, T.; Ali, M. Carbon Capture by Physical Adsorption: Materials, Experimental Investigations and Numerical Modeling and Simulations − A Review. *Appl. Energy* **2016**, *161*, 225−255.

(20) Karimi, M.; Diaz de Tuesta, J. L.; Carmem, C. N.; Gomes, H. T.; Rodrigues, A. E.; Silva, J. A. C. Compost from Municipal Solid Wastes as a Source of Biochar for CO2 Capture. *Chem. Eng. Technol.* **2020**, *43*, 1336−1349.

(21) Weckhuysen, B. M.; Yu, J. Recent Advances in Zeolite Chemistry and Catalysis. *Chem. Soc. Rev.* **2015**, *44*, 7022−7024.

(22) Maurin, G.; Serre, C.; Cooper, A.; Férey, G. The New Age of MOFs and of Their Porous-Related Solids. *Chem. Soc. Rev.* **2017**, *46*, 3104−3107.

(23) Karimi, M.; Rodrigues, A. E.; Silva, J. A. C. Biomass as a Source of Adsorbents for CO2 Capture. *Adv. Bioenergy Microfluid. Appl.* **2021**, 255−274.

(24) Raganati, F.; Miccio, F.; Ammendola, P. Adsorption of Carbon Dioxide for Post-Combustion Capture: A Review. *Energy Fuels* **2021**, *35*, 12845−12868.

(25) Yaghi, O. M.; Li, H. Hydrothermal Synthesis of a Metal-Organic Framework Containing Large Rectangular Channels. *J. Am. Chem. Soc.* **1995**, *117*, 10401−10402.

(26) Hoskins, B. F.; Robson, R. Infinite Polymeric Frameworks Consisting of Three Dimensionally Linked Rod-like Segments. *J. Am. Chem. Soc.* **1989**, *111*, 5962−5964.

(27) Férey, G. Hybrid Porous Solids: Past, Present, Future. *Chem. Soc. Rev.* **2008**, *37*, 191−214.

(28) Zhou, H. C.; Long, J. R.; Yaghi, O. M. Introduction to Metal−Organic Frameworks. *Chem. Rev.* **2012**, *112*, 673−674.

(29) Yu, H.; Wang, X.; Xu, C.; Chen, D. L.; Zhu, W.; Krishna, R. Utilizing Transient Breakthroughs for Evaluating the Potential of Kureha Carbon for CO2 Capture. *Chem. Eng. J.* **2015**, *269*, 135−147.

(30) Adil, K.; Belmabkhout, Y.; Pillai, R. S.; Cadiau, A.; Bhatt, P. M.; Assen, A. H.; Maurin, G.; Eddaoudi, M. Gas/Vapour Separation Using Ultra-Microporous Metal−Organic Frameworks: Insights into the Structure/Separation Relationship. *Chem. Soc. Rev.* **2017**, *46*, 3402−3430.

(31) Liu, J.; Thallapally, P. K.; Mc Grail, B. P.; Brown, D. R.; Liu, J. Progress in Adsorption-Based CO2 Capture by Metal−Organic Frameworks. *Chem. Soc. Rev.* **2012**, *41*, 2308−2322.

(32) Sumida, K.; Rogow, D. L.; Mason, J. A.; McDonald, T. M.; Bloch, E. D.; Herm, Z. R.; Bae, T. H.; Long, J. R. Carbon Dioxide Capture in Metal−Organic Frameworks. *Chem. Rev.* **2012**, *112*, 724−781.

(33) Llewellyn, P. L.; Bourrelly, S.; Serre, C.; Vimont, A.; Daturi, M.; Hamon, L.; de Weireld, G.; Chang, J. S.; Hong, D. Y.; Hwang, Y. K.; Jhung, S. H.; Férey, G. High Uptakes of CO2 and CH4 in Mesoporous Metal-Organic Frameworks MIL-100 and MIL-101. *Langmuir* **2008**, *24*, 7245−7250.

(34) Samanta, A.; Zhao, A.; Shimizu, G. K. H.; Sarkar, P.; Gupta, R. Post-Combustion CO2 Capture Using Solid Sorbents: A Review. *Ind. Eng. Chem. Res.* **2012**, *51*, 1438−1463.

(35) Brandani, F.; Ruthven, D. M. The Effect of Water on the Adsorption of CO2 and C3H8 on Type X Zeolites. *Ind. Eng. Chem. Res.* **2004**, *43*, 8339−8344.

(36) Kizzie, A. C.; Wong-Foy, A. G.; Matzger, A. J. Effect of Humidity on the Performance of Microporous Coordination Polymers as Adsorbents for CO2 Capture. *Langmuir* **2011**, *27*, 6368−6373.

(37) Liu, J.; Wang, Y.; Benin, A. I.; Jakubczak, P.; Willis, R. R.; LeVan, M. D. CO2/H2O Adsorption Equilibrium and Rates on Metal-Organic Frameworks: HKUST-1 and Ni/DOBDC. *Langmuir* **2010**, *26*, 14301−14307.

https://doi.org/10.1021/acs.iecr.2c04150
Ind. Eng. Chem. Res. 2023, 62, 5216−5229

(38) Mouchaham, G.; Cui, F. S.; Nouar, F.; Pimenta, V.; Chang, J. S.; Serre, C. Metal−Organic Frameworks and Water: 'From Old Enemies to Friends'? *Trends Chem.* **2020**, *2*, 990−1003.
(39) Brandt, P.; Nuhnen, A.; Lange, M.; Möllmer, J.; Weingart, O.; Janiak, C. Metal-Organic Frameworks with Potential Application for SO2 Separation and Flue Gas Desulfurization. *ACS Appl. Mater. Interfaces* **2019**, *11*, 17350−17358.
(40) Gu, Y. M.; Qi, H. F.; Sun, T. T.; Liu, X. W.; Qadir, S.; Sun, T. J.; Li, D. F.; Zhao, S. S.; Fairen-Jimenez, D.; Wang, S. D. Insights into the Ultra-High Volumetric Capacity in a Robust Metal-Organic Framework for Efficient C2H2/CO2Separation. *Chem. Mater.* **2022**, *34*, 2708−2716.
(41) Brântuas, P. F.; Henrique, A.; Wahiduzzaman, M.; von Wedelstedt, A.; Maity, T.; Rodrigues, A. E.; Nouar, F.; Lee, U.-H.; Cho, K.-H.; Maurin, G.; Silva, J. A. C.; Serre, C.; Brântuas, P. F.; Henrique, A.; Maity, T.; Silva, J. A. C.; Rodrigues, A. E. Separation of Branched Alkanes Feeds by a Synergistic Action of Zeolite and Metal-Organic Framework. *Adv. Sci.* **2022**, *9*, 2201494.
(42) Cadiau, A.; Lee, J. S.; Borges, D.; Fabry, P.; Devic, T.; Wharmby, M. T.; Martineau, C.; Foucher, D.; Taulelle, F.; Jun, C.-H.; Hwang, Y. K.; Stock, N.; de Lange, M. F.; Kapteijn, F.; Gascon, J.; Maurin, G.; Chang, J.-S.; Serre, C.; Cadiau, A.; Fabry, P.; Devic, T.; Martineau, C.; Foucher, D.; Taulelle, F.; Serre, C.; Lee, J. S.; Hwang, Y. K.; Chang, J.-S.; Jun, C.-H.; Damasceno-Borges, D.; Maurin, G.; de Lange, M. F.; Kapteijn, F.; Gascon, J. Design of Hydrophilic Metal Organic Framework Water Adsorbents for Heat Reallocation. *Adv. Mater.* **2015**, *27*, 4775−4780.
(43) Borges, D. D.; Maurin, G.; Galvao, D. S. Design of Porous Metal-Organic Frameworks for Adsorption Driven Thermal Batteries. *MRS Adv.* **2017**, *2*, 519−524.
(44) Permyakova, A.; Skrylnyk, O.; Courbon, E.; Affram, M.; Wang, S.; Lee, U. H.; Valekar, A. H.; Nouar, F.; Mouchaham, G.; Devic, T.; de Weireld, G.; Chang, J. S.; Steunou, N.; Frère, M.; Serre, C. Synthesis Optimization, Shaping, and Heat Reallocation Evaluation of the Hydrophilic Metal−Organic Framework MIL-160(Al). *ChemSusChem* **2017**, *10*, 1419−1426.
(45) Severino, M. I.; Gkaniatsou, E.; Nouar, F.; Pinto, M. L.; Serre, C. MOFs Industrialization: A Complete Assessment of Production Costs. *Faraday Discuss.* **2021**, *231*, 326−341.
(46) Karimi, M.; Rodrigues, A. E.; Silva, J. A. C. Designing a Simple Volumetric Apparatus for Measuring Gas Adsorption Equilibria and Kinetics of Sorption. Application and Validation for CO2, CH4 and N2 Adsorption in Binder-Free Beads of 4A Zeolite. *Chem. Eng. J.* **2021**, *425*, No. 130538.
(47) Boer, J. H. *The Dynamical Character of Adsorption*, 1st ed.; Oxford press: London, 1953.
(48) Do, D. D. *Adsorption Analysis: Equilibria and Kinetics (With CD Containing Computer Matlab Programs);* 1st ed.; Imperial College Press: London, 1998; Vol. 2.
(49) Ruthven, D. M. *Principles of Adsorption and Adsorption Processes;* 1st ed.; Wiley: New York, 1984.
(50) Sircar, S.; Mohr, R.; Ristic, C.; Rao, M. B. Isosteric Heat of Adsorption: Theory and Experiment. *J. Phys. Chem. B* **1999**, *103*, 6539−6546.
(51) Streb, A.; Mazzotti, M. Adsorption for Efficient Low Carbon Hydrogen Production: Part 1—Adsorption Equilibrium and Breakthrough Studies for H2/CO2/CH4 on Zeolite 13X. *Adsorption* **2021**, *27*, 541−558.
(52) Sircar, S. Linear-Driving-Force Model for Non-Isothermal Gas Adsorption Kinetics. *J. Chem. Soc., Faraday Trans. 1* **1983**, *79*, 785−796.
(53) Zafanelli, L. F. A. S.; Henrique, A.; Karimi, M.; Rodrigues, A. E.; Silva, J. A. C. Single- A Nd Multicomponent Fixed Bed Adsorption of CO2, CH4, and N2in Binder-Free Beads of 4A Zeolite. *Ind. Eng. Chem. Res.* **2020**, *59*, 13724−13734.
(54) Zhao, Q.; Wu, F.; Men, Y.; Fang, X.; Zhao, J.; Xiao, P.; Webley, P. A.; Grande, C. A. CO2 Capture Using a Novel Hybrid Monolith (H-ZSM5/Activated Carbon) as Adsorbent by Combined Vacuum and Electric Swing Adsorption (VESA). *Chem. Eng. J.* **2019**, *358*, 707−717.
(55) Shirzad, M.; Karimi, M. Statistical Analysis and Optimal Design of Polymer Inclusion Membrane for Water Treatment by Co(II) Removal. *Desalination Water Treat.* **2020**, *182*, 194−207.
(56) Myers, R. H.; Montgomery, D. C.; Anderson-Cook, C. M. *Response Surface Methodology : Process and Product Optimization Using Designed Experiments*, 4th ed.; Wiley: New York, 2016.
(57) Henrique, A.; Karimi, M.; Silva, J. A. C.; Rodrigues, A. E. Analyses of Adsorption Behavior of CO 2 , CH 4 , and N 2 on Different Types of BETA Zeolites. *Chem. Eng. Technol.* **2019**, *42*, 327−342.
(58) Li, X.; Zhou, Q.; Yang, H. Ultrafast and Stable Adsorption-Desorption Performance for Recovery of Valuable Rare-Earth Ions Using High-Density Polyacrylic Acid Brush-Grafted Polypropylene Fibers Optimized by RSM Models. *Ind. Eng. Chem. Res.* **2020**, *59*, 7746−7754.
(59) Schiesser, W. *The Numerical Method of Lines : Integration of Partial Differential Equations*, 1st ed.; Elsevier: Amsterdam , 1991.
(60) Borges, D. D.; Normand, P.; Permiakova, A.; Babarao, R.; Heymans, N.; Galvao, D. S.; Serre, C.; de Weireld, G.; Maurin, G. Gas Adsorption and Separation by the Al-Based Metal-Organic Framework MIL-160. *J. Phys. Chem. C* **2017**, *121*, 26822−26832.
(61) Barrer, R. M. *Zeolites and Clay Minerals as Sorbents and Molecular Sieves*; Academic Press, 1978.
(62) Karimi, M.; Shirzad, M.; Silva, J. A. C.; Rodrigues, A. E. Biomass/Biochar Carbon Materials for CO2 Capture and Sequestration by Cyclic Adsorption Processes: A Review and Prospects for Future Directions. *J. CO2 Util.* **2022**, *57*, No. 101890.
(63) Yang, R. T. *Gas Separation by Adsorption Processes*, 1st ed.; Elsevier: New York, 1987.
(64) s
(65) Lin, Y.; Kong, C.; Chen, L. Direct Synthesis of Amine-Functionalized MIL-101(Cr) Nanoparticles and Application for CO2 Capture. *RSC Adv.* **2012**, *2*, 6417−6419.
(66) Cmarik, G. E.; Kim, M.; Cohen, S. M.; Walton, K. S. Tuning the Adsorption Properties of UiO-66 via Ligand Functionalization. *Langmuir* **2012**, *28*, 15606−15613.
(67) Karra, R.; Walton, K. S. Molecular Simulations and Experimental Studies of CO2, CO, and 2 Adsorption in Metal−Organic Frameworks. *J. Phys. Chem. C* **2010**, *114*, 15735−15740.
(68) Yang, Q.; Xue, C.; Zhong, C.; Chen, J. F. Molecular Simulation of Separation of CO2 from Flue Gases in CU-BTC Metal-Organic Framework. *AIChE J.* **2007**, *53*, 2832−2840.
(69) Liu, B.; Smit, B. Comparative Molecular Simulation Study of CO2/N2 and CH4/N2 Separation in Zeolites and Metal−Organic Frameworks. *Langmuir* **2009**, *25*, 5918−5926.
(70) Querejeta, N.; Plaza, M. G.; Rubiera, F.; Pevida, C.; Avery, T.; Tennisson, S. R. Carbon Monoliths in Adsorption-Based Post-Combustion CO2 Capture. *Energy Proc.* **2017**, *114*, 2341−2352.
(71) Shen, Y.; Shi, W.; Zhang, D.; Na, P.; Fu, B. The Removal and Capture of CO2 from Biogas by Vacuum Pressure Swing Process Using Silica Gel. *J. CO2 Util.* **2018**, *27*, 259−271.
(72) Brea, P.; Delgado, J. A.; águeda, V. I.; Gutiérrez, P.; Uguina, M. A. Multicomponent Adsorption of H2, CH4, CO and CO2 in Zeolites NaX, CaX and MgX. Evaluation of Performance in PSA Cycles for Hydrogen Purification. *Microporous Mesoporous Mater.* **2019**, *286*, 187−198.

https://doi.org/10.1021/acs.iecr.2c04150
Ind. Eng. Chem. Res. 2023, 62, 5216−5229